Journal of Chromatography, 646 (1993) 67–80
Elsevier Science Publishers B.V., Amsterdam

CHROMSYMP. 2865

High-performance liquid chromatography of amino acids, peptides and proteins

CXXVI[☆]. Modelling of protein adsorption with non-porous and porous particles in a finite bath

Q.M. Mao, R. Stockmann, I.G. Prince and M.T.W. Hearn*

Department of Biochemistry and Centre for Bioprocess Technology, Monash University, Clayton, Vic. 3168 (Australia)

ABSTRACT

Analytical solutions for a mathematical model describing dynamic adsorption processes of proteins onto non-porous adsorbent particles in a finite bath are presented. The model, based on the Langmuir adsorption isotherm, has been applied to experimental data obtained with affinity and ion-exchange adsorbents. The external film mass transfer resistance, as well as the rate of surface interaction between proteins and adsorbents, have been taken into account. The model has been extended to the case of adsorption onto porous particles by employing a linear driving force approximation for describing mass transfer in the pore fluid. This approach enables the derivation of an effective overall liquid phase mass transfer coefficient, permitting subsequent adaptation of the analytical solutions developed for non-porous particles. The evaluation of the effective liquid phase mass transfer coefficients is also described. Examples of a comparison between predicted and experimental dynamic adsorption curves for both dye-affinity and ion-exchange systems are presented. The application of the model for predicting the optimum operating conditions is discussed.

INTRODUCTION

Advances in biotechnology continue to see more proteins, whether natural or recombinant, being purified at commercial scale. Various adsorption methods, and in particular chromatography, typically form a central part of protein purification processes. Porous sorbents are normally used including softgel materials as well as rigid particles such as silica-based sorbents. Recently applications where non-porous particles may have advantage have gained more attention, including examples involving silica-based affinity chromatography [1,2], silica-based ion-exchange chromatography [3,4], silica-based reversed-phase chromatography [5], metal ion compounds immobilised onto agarose beads [6], as well as new types of ceramic particles [7]. However, theoretical treatment specifically developed for non-porous particle systems are very limited [8,9].

The various chromatographic processes normally involve a four-stage (adsorption, washing, elution and regeneration) operation in sequence in a packed bed configuration. In cases where the feed concentration is very low, large quantities of liquid have to be processed. The adsorption time to make full use of the column capacity may become very long in these circumstances, as flow-rates are constrained by pressure-drop considerations. This operating time can be reduced by carrying out the adsorption stage in a stirred

* Corresponding author.
☆ For Part CXXV, see ref. 27.

0021-9673/93/$06.00

tank (finite bath) [10]. Also, with fermentation broth or biological extracts containing cell debris and other solid contaminants, a stirred tank may be preferable for the adsorption stage to avoid the clogging problems experienced with a packed bed. Certainly, for laboratory studies of adsorption processes, a finite bath is often a simple and chapter tool to use.

An extensive literature of experimental studies of protein adsorption kinetics and equilibrium behaviour in finite baths for both affinity and ion-exchange sorbents is available [9,11–16]. Various mathematical models have also been developed to describe the adsorption behaviour of proteins in a finite bath [9,11,13,15,17–19].

These existing models can be classified into two groups. In the first group a single factor is assumed to be the rate limiting step, either pore diffusion [18] or surface interaction [11,17]. This simplification allows analytical solutions to be obtained. In the second group, the models are more rigorous as all of the possible important rate-limiting steps are considered, but various numerical methods are necessary to obtain solutions [9,13,15,19]. As most protein adsorption systems display non-linear adsorption isotherm characteristics, this behaviour is incorporated in the models in both groups, often in the form of a Langmuir isotherm.

All the various models have been developed for porous particles, although the Group-2 models could be modified to solve non-porous particle problems. For adsorption in a finite bath, only one model [9] has been explicitly developed for non-porous particles with a numerical solution used. The numerical methods that have been necessary to solve the Group-2 models often result in excessive computation time [13] and hence simplification of the model has often been necessary [20] to allow practical application.

This paper presents a model which describes dynamic adsorption processes of proteins onto non-porous adsorbent particles in a finite bath. The effects of both surface interaction and film mass transfer have been addressed. Due to the absence of pore diffusion, analytical solutions for the model and its two simplified cases were derived. The model was then extended to cover the case of porous particles by using a linear driving force approximation to describe the pore diffusion process.

MODEL DEVELOPMENT

Adsorption with non-porous particles

The batch adsorption model (BchAM) has been developed to describe the adsorption behaviour of proteins in a finite bath, initially for non-porous particles. In a finite bath a volume of the fluid containing the solute protein (adsorbate) of interest is brought into contact with a quantity of adsorbent at time zero in a well-mixed vessel. Interaction is then allowed to occur for a period of time as equilibrium is approached.

The overall mass balance for the adsorption with non-porous particles in a finite bath can be expressed as

$$\varepsilon C + (1 - \varepsilon)q = \varepsilon C_T \quad (1)$$

where C is the adsorbate concentration in the bulk of the liquid phase, q is the adsorbate concentration on the solid phase, and ε is the volume fraction of liquid phase in the finite bath. The variable C_T is the equivalent adsorbate concentration when the total amount of the adsorbate in the system is assumed only in the liquid phase, and C_T can be calculated from

$$C_T = C_0 + R_v q_0 \quad (2)$$

where C_0 is the initial adsorbate concentration in the liquid phase, q_0 is the initial adsorbate concentration in the solid phase, and R_v [$= (1 - \varepsilon)/\varepsilon$] is the volume ratio of the solid phase to the liquid phase. For adsorption with fresh or regenerated adsorbent particles, $q_0 = 0$ and $C_T = C_0$. For washing the elution stages, $C_0 = 0$ and $C_T = R_v q_0$.

The differential form of eqn. 1 then can be expressed as

$$\frac{dC}{dt} + R_v \frac{dq}{dt} = 0 \quad (3)$$

The basic assumptions for rate limiting steps in the adsorption process in a finite bath are the

same as those used in the non-porous particle adsorption model for a packed bed [8]. These assumptions are: (a) The transport of adsorbate from the bulk fluid to the surface of the particle can be described by a film resistance mechanism. (b) The interaction between the adsorbate and the adsorption site at the particle surface is described by a Langmuir-type model. In addition, as has been implied in the above equations, the finite bath is assumed to be well mixed, therefore the concentration of the adsorbate in the liquid phase is uniform throughout the finite bath. As in the case with the non-porous particle adsorption model, the transport of adsorbate from the bulk fluid to the surface of the particle is described by a film resistance mechanism

$$\frac{dq}{dt} = aK_f(C - C^*) \tag{4}$$

where a ($=3/R_0$) is the interfacial area per unit volume of the adsorbent particles, R_0 is the radius of the particle, K_f is the liquid film mass transfer coefficient, and C^* is the intermediate concentration of the adsorbate in the liquid phase at the surface of the particles.

The interaction between the adsorbate and the immobilised ligand at the particle surface is described by the second-order reversible equation

$$\frac{dq}{dt} = k_1[(q_m - q)C^* - K_d q] \tag{5}$$

where k_1 is the forward interaction rate constant, q_m is the maximum adsorption capacity of the immobilised ligand, and K_d is the adsorption equilibrium constant. At equilibrium, eqn. 5 becomes the Langmuir isotherm equation.

Eliminating C^*, q and its derivative from eqns. 2, 3, 4 and 5, the rate of change of C with time can be written as follows

$$-\left(\frac{1}{M} + \frac{1}{k_1}\right)\frac{dC}{dt} = (C - x_1)(C - x_2) \tag{6}$$

where

$$M = \frac{A}{R_v q_m - C_T + C} \tag{7}$$

and

$$A = aK_f R_v \tag{8}$$

x_1 and x_2 are the roots of quadratic equation

$$C^2 - BC - K_d C_T = 0 \tag{9}$$

where

$$B = C_T - R_v q_m - K_d \tag{10}$$

and

$$x_1 = \frac{1}{2}[B + \sqrt{B^2 + 4K_d C_T}]$$

$$x_2 = \frac{1}{2}[B - \sqrt{B^2 + 4K_d C_T}] \tag{11}$$

At equilibrium, the left hand side of eqn. 6 becomes zero and eqn. 6 becomes eqn. 9. Hence the positive root of eqn. 9, x_i, is the concentration of the adsorbate in the liquid phase when the finite bath system has reached equilibrium.

Eqn. 6 can be directly integrated to yield

$$\left(C_T - R_v q_m - \frac{A}{k_1}\right)\ln\left(\frac{C - x_1}{C - x_2}\cdot\frac{C_0 - x_2}{C_0 - x_1}\right) - x_1 \ln\left(\frac{C - x_1}{C_0 - x_1}\right) + x_2 \ln\left(\frac{C - x_2}{C_0 - x_2}\right) = A(x_1 - x_2)t \tag{12}$$

Eqn. 12 is the solution of the batch adsorption model from which the concentration–time profile for a given system can be calculated. In this equation as well as in eqn. 6 both the film mass transfer and surface interaction rates are considered finite.

As with our earlier investigations with the non-porous particle adsorption model [8], it is possible to consider two simplified cases. Firstly when $k_1 \to \infty$, the external mass transfer becomes the rate controlling step. As a result, when the forward rate constant for adsorption is very large eqn. 6 becomes

$$-\frac{1}{M}\cdot\frac{dC}{dt} = (C - x_1)(C - x_2) \tag{13}$$

and the integrated result is

$$(C_T - R_v q_m)\ln\left(\frac{C - x_1}{C - x_2}\cdot\frac{C_0 - x_2}{C_0 - x_1}\right) - x_1 \ln\left(\frac{C - x_1}{C_0 - x_1}\right) + x_2 \ln\left(\frac{C - x_2}{C_0 - x_2}\right) = A(x_1 - x_2)t \tag{14}$$

Because eqn. 13 implies that equilibrium exists between the adsorbate and the adsorbate–ligand complex at each point on the particle surface, this mass transfer controlling case of the batch adsorption model was abbreviated as BchAME.

Secondly, if $K_f \rightarrow \infty$ then the surface interaction (second-order kinetics) is considered as the rate controlling step. As a result, $A \rightarrow \infty$ and $1/M \rightarrow 0$. Hence, when the liquid film mass transfer coefficient K_f becomes dominant eqn 6 becomes

$$-\frac{1}{k_1}\cdot\frac{dC}{dt} = (C - x_1)(C - x_2) \quad (15)$$

and the integrated form is

$$-\frac{1}{k_1}\ln\left(\frac{C - x_1}{C - x_2}\cdot\frac{C_0 - x_2}{C_0 - x_1}\right) = (x_1 - x_2)t \quad (16)$$

This case can be designated as the kinetic controlling case of the batch adsorption model abbreviated as BchAMK. In this case, the concentration of the adsorbate in the liquid phase as a function of time then can be expressed as

$$C = \frac{x_1(C_0 - x_2) - x_2(C_0 - x_1)\,e^{(x_2 - x_1)k_1 t}}{(C_0 - x_2) - (C_0 - x_1)\,e^{(x_2 - x_1)k_1 t}} \quad (17)$$

which produces a similar result to that derived from the equations of Horstmann *et al.* [11].

Eqn. 17 can be used directly to calculate the time–concentration profile. In the cases where the value of the liquid mass transfer coefficient K_f is finite, *i.e.* eqn. 12 or 14 is required, a bisectional method can be adopted to calculate the profiles. For an actual process, eqns. 12, 14 or 16 can be used to estimate the time required to reach a predetermined final concentration in the finite bath.

Adsorption with porous adsorbent particles

The batch adsorption model can be modified for the adsorption behaviour with porous particles. A linear driving force approximation was used to describe the mass transfer of the adsorbate in the liquid from the entrance of the pores at the external surface to the particle internal surface. With this approximation the pore fluid can be treated as a mass transfer medium rather than a separate phase thus enabling it to be combined with the bulk fluid in the overall mass balance. In order to extend the batch adsorption model to porous sorbents, the mass balance, rate-limiting steps and the mass transfer coefficients must be considered.

Mass balance

In an actual process, the pores of the adsorbent particles are normally filled with buffer liquid before the adsorption process starts. Hence, the overall mass balance is

$$\varepsilon C + (1 - \varepsilon)\varepsilon_p C_p + (1 - \varepsilon)(1 - \varepsilon_p)_q = [\varepsilon + (1 - \varepsilon)\varepsilon_p]C_T \quad (18)$$

where C_p is the adsorbate concentration in the pore fluid and ε_p is the particle void fraction. Other symbols are the same as defined in eqn. 1. The unit of q is taken as the mass per unit volume of solid. In this case, the value of C_T is given by

$$C_T = \frac{\varepsilon C_0 + (1 - \varepsilon)\varepsilon_p C_{p0} + (1 - \varepsilon)(1 - \varepsilon_p)q_0}{\varepsilon + (1 - \varepsilon)\varepsilon_p} \quad (19)$$

For adsorption with fresh or regenerated adsorbent particles, $q_0 = 0$, $C_{p0} = 0$ and C_T can be written as

$$C_T = \frac{\varepsilon C_0}{\varepsilon + (1 - \varepsilon)\varepsilon_p} \quad (20)$$

For washing stage, $C_0 = 0$ and C_T becomes

$$C_T = \frac{(1 - \varepsilon)\varepsilon_p C_{p0} + (1 - \varepsilon)(1 - \varepsilon_p)q_0}{\varepsilon + (1 - \varepsilon)\varepsilon_p} \quad (21)$$

As the volume of pore fluid is normally very small in comparison with the volume of bulk fluid, it may be neglected or lumped with the bulk fluid. Hence, two simplifying options can be considered.

Option 1. Neglecting the pore fluid (*i.e.* let $\varepsilon_p = 0$), eqn. 18 becomes the same as for the non-porous particles (eqn. 1). The differential form of the equation then becomes the same as eqn. 3, with the same volume ratio, $R_v = (1 - \varepsilon)/\varepsilon$.

Option 2. When the pore fluid is lumped with the bulk fluid, $C_p = C$, and eqn. 18 becomes

$$[\varepsilon + (1-\varepsilon)\varepsilon_p]C + (1-\varepsilon)(1-\varepsilon_p)q = [\varepsilon + (1-\varepsilon)\varepsilon_p]C_T \quad (22)$$

However, the differential form of eqn. 22 is

$$\frac{dC}{dt} + R_v \frac{dq}{dt} = 0 \quad (23)$$

which is the same as eqn. 3, except the volume ratio of the solid phase to the liquid phase, R_v, becomes

$$R_v = \frac{1 - [\varepsilon + (1-\varepsilon)\varepsilon_p]}{\varepsilon + (1-\varepsilon)\varepsilon_p} \quad (24)$$

Rate-limiting steps

The rate-limiting steps in an adsorption process are the mass transfers and the surface interaction. As discussed previously [16], for protein adsorption processes, the effect of both steps should be taken into account. For porous particles, as the internal surface area is normally much greater than the external surface area, the effect of the external surface area may be neglected (in the case where the external surface are is less than, *e.g.* 1.0% of the total surface area) or lumped with the internal surface area in the modelling process. Hence the model proposed here assumes that the surface interaction will predominantly occur when the adsorbate reaches the internal surface of the particles.

Mass transfer. The model considers that the transport of adsorbate from the bulk fluid to the internal surface of the particle occurs in two stages. First the adsorbate diffuses through a thin film to reach the external surface of the particle where the entrances to the pores are located; then the adsorbate diffuses through the pore fluid, which is stagnant, to reach the particle internal surface where the surface interaction between the adsorbate and the ligand will occur. As both the liquid film on the external surface of the particle and the pore fluid are the media for mass transfer, both processes may be described by a linear driving force approximation, and so as the overall mass transfer process. Therefore, the mass transfer rate of the adsorbate from the bulk fluid to the internal particle surface can be expressed as

$$N = K_f(C - C^*) = K_p(C^* - C_i) = K_e(C - C_i) \quad (25)$$

where N is the mass flux of the adsorbate into the particle, K_f is the liquid film mass transfer coefficient, K_p is the apparent pore fluid mass transfer coefficient, and K_e is the overall effective liquid phase mass transfer coefficient. C^* is the intermediate concentration of the adsorbate in the liquid phase at the external surface of the particles, and C_i is the intermediate concentration of the adsorbate in the liquid phase at the internal surface of the particles.

Assuming that the volume of the liquid film is negligible, and there is no accumulation of the adsorbate in the pore fluid, the rate of change in the concentration of the adsorbate in the solid phase then must equal to the rate of mass transfer, hence

$$\frac{dq}{dt} = aK_f(C - C^*) = aK_p(C^* - C_i) \quad (26)$$

where the term $a = (3/R_0)$ is the external surface area per unit volume of the adsorbent particles and R_0 is the radius of the particle.

From eqns. 25 and 26 the following form of the rate of change of adsorbate concentration can be written

$$\frac{dq}{dt} = aK_e(C - C_i) \quad (27)$$

and

$$\frac{1}{K_e} = \frac{1}{K_f} + \frac{1}{K_p} \quad (28)$$

Eqn. 28 clearly shows that the overall resistance to the mass transfer is the sum of the resistance in the liquid film and the resistance in the pore fluid.

Surface interaction. The interaction between the adsorbate and the immobilised ligand at the internal particle surface can be described by the second-order reversible equation

$$\frac{dq}{dt} = k_1[(q_m - q)C_i - K_d q] \quad (29)$$

where k_1 is the forward interaction rate constant, q_m is the maximum adsorption capacity of the immobilised ligand, and K_d is the adsorption

equilibrium constant. This equation is identical with eqn. 5 except that C^* is replaced by C_i, the concentration of adsorbate in the liquid phase at internal surface of the particles.

Determination of the mass transfer coefficients

As in the case with the non-porous particles, the liquid film mass transfer coefficient K_f can be calculated from literature correlations [13,21]. The apparent pore liquid mass transfer coefficient K_p may be expressed as an effective pore diffusivity over an average effective diffusion path length

$$K_p = \frac{\lambda^* D_e}{\sigma R_0} \tag{30}$$

where D_e is the effective pore diffusivity, and λ^* is an area factor. The apparent pore liquid mass transfer coefficient K_p is based on the external surface area a, whilst D_e is based on the total area perpendicular to the direction of diffusion, a^* which is less than the total internal surface area per unit volume of the particle but much bigger than a (λ^* is the ratio of a^* to a). The term σR_0 is the average effective diffusion path length which is expressed as a linear function of the particle radius R_0. The effective diffusivity D_e, according to the random pore model [22], can be estimated from

$$D_e = D_M \varepsilon_p^2 \tag{31}$$

where D_M is the free molecular diffusivity which may be calculated from a literature correlation [23].

The solution of the model with porous adsorbents

Eliminating C_i, q and its derivative from eqns. 18, 23, 27 and 29, the following form of the concentration equation can be written as

$$-\left(\frac{1}{M} + \frac{1}{k_1}\right)\frac{dC}{dt} = (C - x_1)(C - x_2) \tag{32}$$

which is identical with eqn. 6. As the only difference between this option and the non-porous particle case is that K_f has been replaced by K_e, the solutions given by eqns. 9 and 12 can be directly applied with

$$A = aK_eR_v \tag{33}$$

EXPERIMENTAL

Data obtained on protein adsorption to two dye-affinity supports and three ion-exchange resins were used in validating the model. The properties of these adsorbents are listed in Table I. The information on the physical characteristics of the three anion-exchange resins (DEAE-Sepharose FF, DEAE-Trisacryl M and DEAE-Fractogel 650 M) is from Johnston and Hearn [14,16]. The data on the Fractogel HW55–Cibacron Blue F3GA system were reported by John-

TABLE I

PROPERTIES OF ION-EXCHANGE AND AFFINITY SUPPORTS

Support	Particle size (μm)	Porosity	q_m (mg/ml)	K_d (mg/ml)
Fractogel HW55–Cibacron Blue F3GA	33	0.4	0.4[a]	0.019[a]
Polygosil 300-2540–Cibacron Blue F3GA	25–40	0.68	93[b]	0.006[b]
DEAE-Sepharose FF	45–165	0.65	110[a]	0.0833[a]
DEAE-Trisacryl M	40–80	0.49	140[a]	0.0179[a]
DEAE-Fractogel 650 M	45–90	0.28	40[c]	0.0105[c]

[a] For HSA.
[b] For lysozyme.
[c] For ferritin.

ston [24]. The silica support used (Polygosil 300-2540, Macherey–Nagel, Düren, Germany) was activated with 3-mercaptopropyltriethoxysilane (MPTS). The Cibacron Blue F3GA dye was then bound to the thiol group of the immobilised silane. The detailed procedure for this surface modification has been reported by Wirth *et al.* [2]. Human serum albumin (HSA), lysozyme and ferritin were used as model proteins. The bath system set-up and experimental procedure are the same as previously described in the studies from our laboratory [12,14]. The only exception is in the case with Polygosil 300-2540, where a modified bath with a much larger sampling filter was used in the bath to prevent the deposition of small particles.

RESULTS AND DISCUSSION

Examination of the effect of rate-controlling parameters

The rate-controlling parameters are the most important factors in determining the kinetic characteristics of an adsorption system. The two main types of rate-controlling parameters, the surface interaction rate constants, and the liquid phase mass transfer coefficients, have all been included in the batch adsorption model. The two simplified cases of the model, however, consider only one type of parameter as being rate limiting. Examination of the shape of the concentration–time profiles predicted by the different cases of the model will therefore offer useful knowledge of the system. Simulations have shown that in some situations, the adsorption profiles do differ significantly.

Fig. 1 shows the concentration–time profiles for human serum albumin adsorption to a DEAE-Trisacryl M system predicted by the three cases of the model. For the purpose of comparison, a curve of best fit to the same hypothetical data points (the small square symbol) was obtained for each case of the model, by adjusting the respective rate constant or mass transfer coefficient. It can be seen that neither of the two simplified cases produced an accurate profile. The mass transfer controlling case (BchAME) predicted a slower adsorption rate

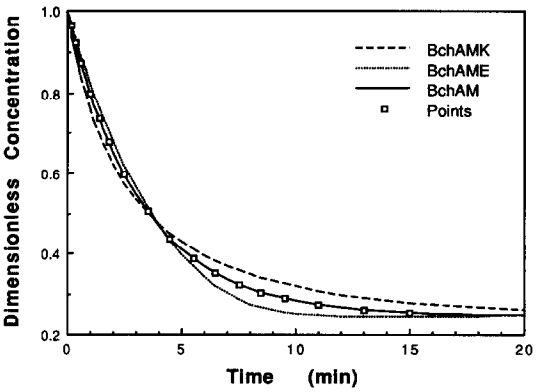

Fig. 1. Kinetic profiles predicted by the three options of the model for the adsorption of HSA to DEAE-Trisacryl M ion-exchange resin. BchAM = The complete batch adsorption model; BchAME = the mass transfer controlling case; BchAMK = the kinetic controlling case.

over the early stage of the process, with the predicted profile reaching equilibrium much faster than the other cases. On the other hand, the surface interaction controlling case (BchAMK) predicted a faster adsorption rate for the initial stage, but reached equilibrium much slower. Only the complete model (BchAM) which incorporates both the mass transfer and the surface interaction provided good fit for the data set in this particular case with HSA.

By using the rate-controlling parameters extracted in simulating the adsorption stage, the concentration–time profiles of the washing stage (washing profile) can be generated. One example of a set of such washing profiles for the same system as in Fig. 1 is shown in Fig. 2, with $k_1 = 0.024$ ml/mg s and $K_e = 1.3 \cdot 10^{-5}$ m/s for the complete model (BchAM), $k_1 = 0.0093$ ml/mg s for the kinetic controlling case (BchAMK), and $K_e = 7.73 \cdot 10^{-6}$ m/s for the mass transfer controlling case (BchAME). Other parameters used for the simulations shown in Figs. 1 and 2 are listed in Table II. The system was assumed to contain the same amount of protein (HSA) at the beginning of the washing stage for all the three cases. The profiles are certainly different, with the mass transfer controlling case predicting the fastest processing rate, and the kinetic controlling case the slowest.

In the above examples, because the difference between the profiles predicted are significant, the

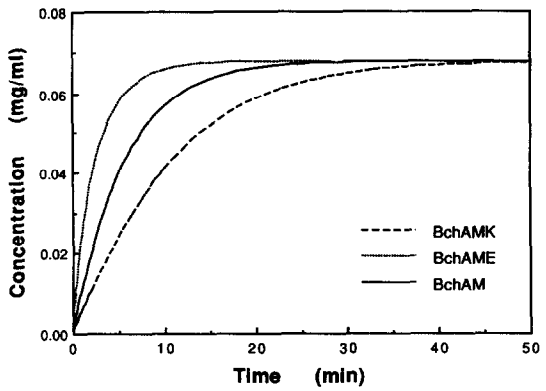

Fig. 2. Concentration–time profiles for the washing stage (washing profile) predicted by the three options of the batch model for HSA-laden DEAE-Trisacryl M resin. (For the abbreviations see legend of Fig. 1.)

values for both k_1 and K_e can be extracted simultaneously by achieving a best fit to the experimental concentration–time curve with the predictions of the complete batch adsorption model. However, under certain operating conditions, the difference between predicted profiles may not be significant enough to warrant a discrimination of the different parameter sets used. This finding suggests that in some situations a simplified model may be sufficient in simulating experimental data, and offers an explanation why the kinetic controlling model sometimes adequately fits the experimental curve as noted by Chase [17]. The situation nevertheless precludes determination of the true values of these rate-controlling parameters.

For non-porous particles, the effective liquid phase mass transfer coefficient K_e contains only one parameter, the liquid film mass transfer coefficient K_f, which may be independently estimated from literature correlations [13,21]. Therefore, the surface interaction rate constant k_1 can be determined. For porous particles, because the apparent pore fluid mass transfer coefficient K_p, which constitutes part of K_e, is difficult to estimate, there is no easy way to solve this problem. A value of k_1 determined from a non-porous particle system with the same protein–ligand combination may have to be used to determine the value of K_e. An alternative procedure involves finding a set of experimental conditions, which will show a significant deviation between the profiles predicted, from computer simulation before the actual experiment. This approach can also be used with a non-porous particle system to evaluate the applicability of the existing correlations for estimating K_f.

Comparison of model prediction with experimental profiles

The predicted concentration–time profiles were compared with experimental adsorption data and the results are shown in Figs. 3–7. In these figures, the points are experimental data and the lines are the model prediction. The

TABLE II

PARAMETERS FOR COMPUTER SIMULATION

Figure No.	C_0 (mg/ml)	R_v	Q_m (mg/ml)	K_d (mg/ml)	K_e (m/s)	k_1 (ml/mg s)
1, 2	0.7	0.00417	140	0.0179	$1.3 \cdot 10^{-5}$	0.024
8	0.05 0.4 0.8	0.005	110	0.0833	$9.6 \cdot 10^{-6}$	0.02
9	0.065	0.0025 0.005 0.01 0.02	110	0.0833	$4.4 \cdot 10^{-6}$	0.5
10, 11, 12	0.1	0.0002–0.2	110	0.0833	$2.4 \cdot 10^{-6}$	0.2

TABLE III

PARAMETERS USED IN SIMULATING EXPERIMENTAL DATA

Figure No.	C_0 (mg/ml)	R_v	K_e (m/s)	k_1 (ml/mg s)
3	0.01	0.0753	$3.03 \cdot 10^{-7}$	0.144
4	0.065	0.0036	$2.86 \cdot 10^{-5}$	0.0153
	0.093		$3.40 \cdot 10^{-5}$	0.019
5	0.0522	0.0042	$1.42 \cdot 10^{-5}$	0.011
6	0.1044	0.0038	$1.25 \cdot 10^{-6}$	0.0036
7	0.0273	0.0048	$1.98 \cdot 10^{-5}$	0.0425
	0.0482	0.0040	$4.82 \cdot 10^{-6}$	0.0185

Note: the K_e values were for the mass transfer controlling case (BchAME), and the k_1 values were for the kinetic controlling case (BchAMK).

properties of the adsorbents are listed in Table I and the parameters used in simulating the profiles are listed in Table III. Dimensionless concentrations, which are the ratio of the measured concentration to the initial concentration, were used in these figures, except in Fig. 4 where measured concentration values were used of the purpose of clarity.

Data of the adsorption of HSA to a dye affinity system, Fractogel HW55–Cibacron Blue F3GA support, are plotted in Fig. 3. The agreement with the predicted profile is good. The comparison with the adsorption of HSA to a weak anion-exchanger DEAE-Sepharose FF

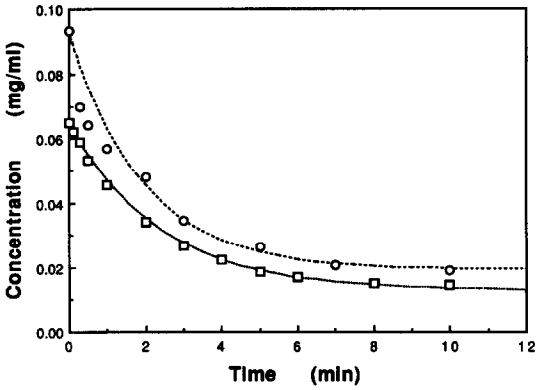

Fig. 4. Theoretical and experimental concentration curves for the adsorption of HSA to a weak anion-exchange resin DEAE-Sepharose FF. (□) $C_0 = 0.065$ mg/ml; (○) $C_0 = 0.093$ mg/ml.

resin is shown in Fig. 4 for two initial protein concentration values. The agreement with $C_0 = 0.065$ mg/ml data is good. For $C_0 = 0.093$ mg/ml data, the model predicted a slower adsorption rate at the early stage of the process. A similar trend is shown in Fig. 5, for adsorption of HSA with DEAE-Trisacryl M.

Fig. 6 shows the result for the adsorption of ferritin with the ion-exchange resin DEAE-Fractogel 650 M. The predicted profile approaches equilibrium faster than the experimental profile. One possible reason to this discrepancy is that the actual diffusion process of this protein molecule in the pore fluid involves a non-linear behaviour, therefore the simple linear driving

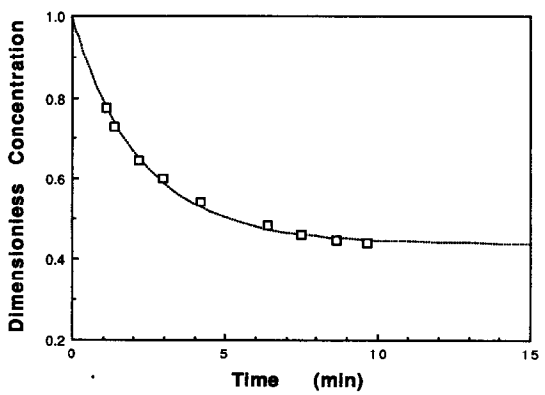

Fig. 3. Theoretical and experimental concentration curves for the adsorption of HSA to the Fractogel HW55–Cibacron Blue F3GA supports.

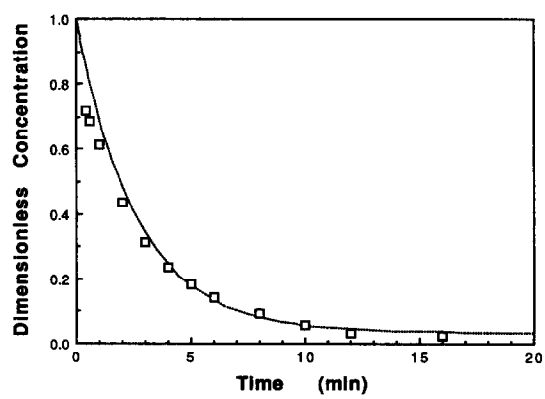

Fig. 5. Theoretical and experimental concentration curves for the adsorption of HSA to a weak anion-exchange resin DEAE-Trisacryl M.

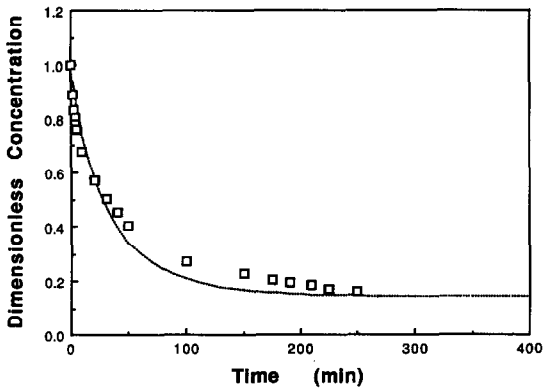

Fig. 6. Theoretical and experimental concentration curves for the adsorption of ferritin to DEAE-Fractogel 650 M.

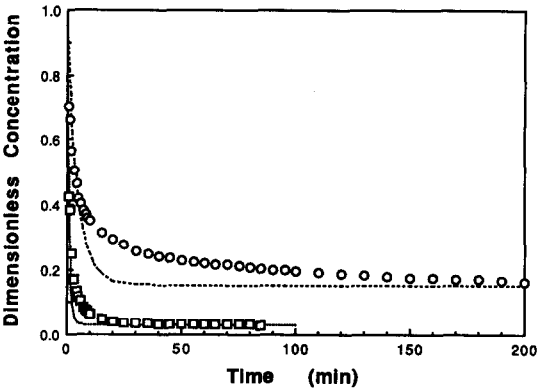

Fig. 7. Theoretical and experimental concentration curves for the adsorption of lysozyme to Cibacron Blue F3GA-modified Polygosil 300-2540. (○) $C_0 = 0.0482$ mg/ml; (□) $C_0 = 0.0273$ mg/ml.

force approach used in the batch adsorption model can not describe this phenomenon accurately. As Ferritin is a large macromolecule (Mr 440 000), it is reasonable to assume that pore diffusion resistance would be a major rate-controlling factor. Hence the approximation used in the model would affect the resulted profile significantly. The effect of pore diffusion resistance can be seen from the effective liquid phase mass transfer coefficients, K_e, derived by the mass transfer controlling case, as shown in Table III. The value of K_e for ferritin is at least an order of magnitude smaller than that for HSA adsorbed by a similar ion-exchange resin. Because the difference between the profiles predicted by the three cases of the model are within the range of variation of the experimental data points in these figures, there is not sufficient justification to determine a single set of K_e and k_1 values for each experimental curve. Therefore the values presented in Table III were determined by the mass transfer controlling case (for K_e) and the kinetic controlling case (for k_1). These values are the lower boundaries of the possible K_e and k_1 values in the complete model.

Fig. 7 shows the profiles for the adsorption of lysozyme to a dye-affinity sorbent, Cibacron Blue F3GA-modified Polygosil 300-2540. The difference between the experimental and predicted profiles is obvious. A possible explanation for the discrepancy is the non-specific binding of lysozyme to the silica surface, which will have a different surface interaction rate. It was also possible that some lysozyme molecules may bind to the already bound lysozyme instead of the ligand. The self aggregation of lysozyme and other proteins in such systems is well documented [25,26], however the role of surface aggregation with this sorbent system requires further investigation. The effect of slow pore diffusion should be small, considering the large pore size (300 nm) of the silica-sorbent used in this case. However, the examples in Figs. 6 and 7 shows that an extended model incorporating all

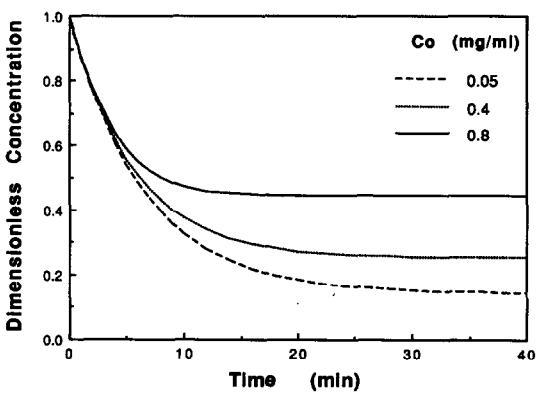

Fig. 8. Effect of initial protein concentration on the kinetic profiles predicted by the batch model for the adsorption of HSA to DEAE-Sepharose FF.

these secondary effects is required to be used for the precise simulation of these systems.

Study of the effect of operating parameters

One of the valuable applications an adsorption model can offer is to predict the effect of changes to various system parameters on the performance of a particular system through computer simulation. As the isotherm parameters and rate-limiting parameters are largely determined by the particular protein–adsorbent combination and their environment (such as temperature, pH and ionic strength), the parameters which can be varied during an experimental study are the operating parameters. The effect of variation of the initial concentration C_0, is shown in Fig. 8 and the solid to liquid volume ratio R_v, is shown in Fig. 9 for an ion-exchange system. The parameters used are listed in table II. In Fig. 8 it can be seen that the change in C_0 mainly affects the final equilibrium concentrations of the system. The effect on the rate of adsorption becomes significant only as equilibrium is approached. The initial part of the concentration–time profiles are almost identical. In contrast, the shape of the profiles is more sensitive to the variation of R_v, as shown in Fig. 8. Both the adsorption rate and the final liquid phase concentration (at equilibrium), are strongly affected by the change in R_v. Hence the effect of R_v should be further studied in determining the optimum operating conditions.

Selection of the optimum operating conditions

To achieve a high production rate and a high yield is important for any commercial process. For the case of protein adsorption in a finite bath, computer simulation with the batch adsorption model was carried out to determine the optimum operating conditions. In the simulation, the yield was defined as the amount of protein adsorbed as the percentage of total protein in the initial solution when the process started. The production rate was defined by dividing the total amount of protein adsorbed when a predetermined value of yield was reached, with the amount of sorbent in the system, and with total processing time. The total processing time is defined as the sum of adsorption time required to achieve a certain yield, and any preparation time associated with the adsorption stage. The preparation time used in the present simulation was set at ten minutes.

Fig. 10 shows the change of processing time to reach 70, 80 and 90% yield, as a function of the solid phase volume ratio R_v. The processing time increases almost linearly with the decrease of R_v value on a log–log scale. Longer time is required to reach higher yield for the same solid to liquid ratio. When the processing time exceeds *ca.* 30

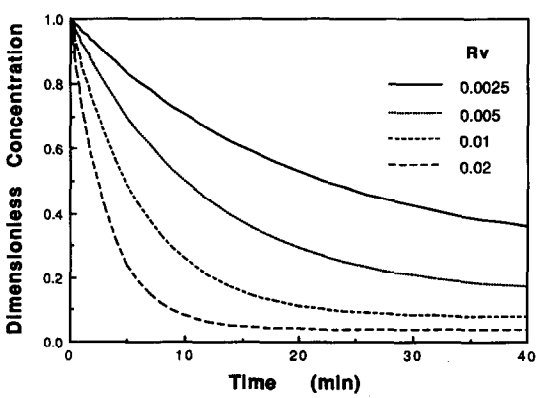

Fig. 9. Effect of solid–liquid volume ratio (R_v) on the kinetic profiles predicted by the batch model for the adsorption of HSA to DEAE-Sepharose FF.

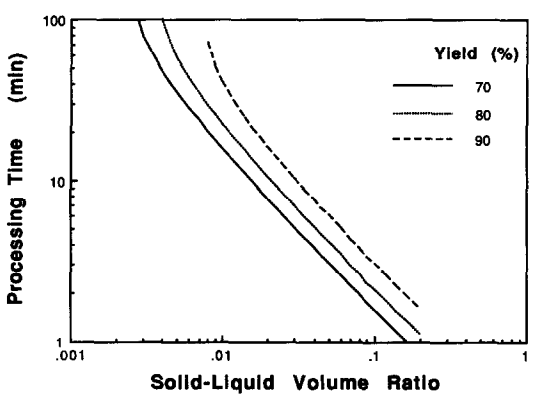

Fig. 10. Processing time as a function of solid–liquid volume ratio and the required yield for the adsorption of HSA to DEAE-Sepharose FF.

min in this example, however, each curve becomes asymptotic towards a limiting R_v value, beyond which the required yield can not be achieved due to the equilibrium restriction, and the processing time approaches infinity at this point.

For each yield requirement, a particular value of R_v was found, which will offer the maximum production rate, as shown in Fig. 11. At 70% yield, the maximum production rate is more than 50% higher than the condition requiring 90% yield. However, for R_v values in the range of 0.03 to 0.05, the variation in the yield shows almost no influence to the production rate. At larger values of R_v, higher production rate is associated with higher yield.

Fig. 12 shows the adsorbent capacity utilised as a function of solid–liquid volume ratio at the three yield values. The capacity utilisation is defined as the ratio of the amount of protein adsorbed per unit adsorbent to the maximum capacity of the adsorbent (Q/Q_m). In the range up to a minimum value of R_v for each curve, a linear relationship exists on a log–log scale. It should be pointed out that the sorbent capacity utilisation in a finite bath is normally low, as a large drop of adsorbate concentration in the liquid phase is often required. In the present simulation, the capacity used, when the maximum production rate is achieved, is in the range of 0.06 to 0.13 depending on the yield required.

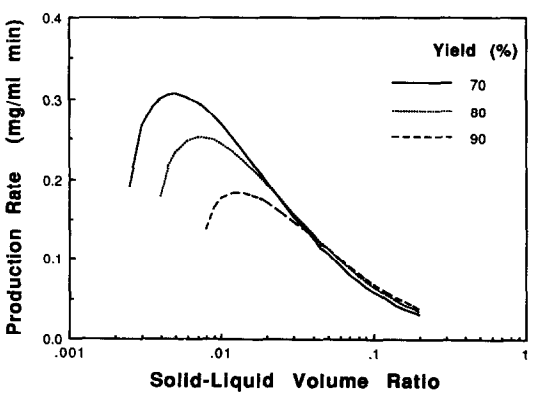

Fig. 11. Production rate (mass of protein adsorbed per unit volume of adsorbent per unit time) as a function of solid–liquid volume ratio and the required yield, for the adsorption of HSA to DEAE-Sepharose FF.

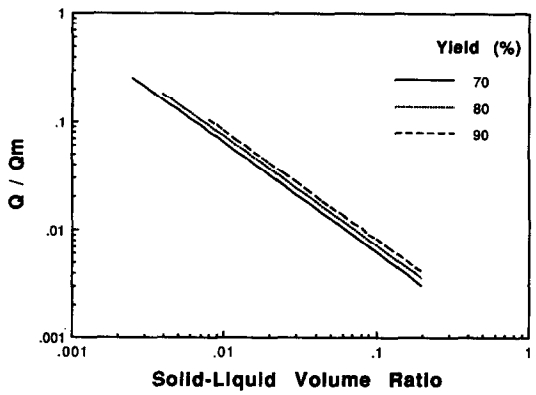

Fig. 12. Adsorbent capacity utilised (expressed as the ratio of the amount adsorbed, Q, to the maximum capacity, Q_m) as a function of solid–liquid volume ratio and the required yield, for the adsorption of HSA to DEAE-Sepharose FF.

CONCLUSIONS

A batch adsorption model (BchAM) has been developed to describe the dynamic adsorption processes of proteins on to non-porous adsorbent particles in a finite bath. The model has been further extended to describe the adsorption processes with porous particles in a finite bath with a linear driving force approximation. An analytical solution has been found. By using an effective liquid phase mass transfer coefficient, the solution can be applied to both non-porous and porous particles. Good agreement was obtained when predicted concentration–time profiles were compared with experimental data for protein adsorption to both dye-affinity and ion-exchange systems. Experimental evidence also suggested that in the cases where pore diffusion is a major rate-limiting factor, or a complicated adsorption kinetics exists, more comprehensive models should be used. For the systems where this model can be applied, the described approach offers an easy and fast solution in determining the adsorption rate and mass transfer coefficients. The model may prove especially suitable for process simulation and process

optimisation where a large amount of computation is often necessary.

ACKNOWLEDGEMENTS

These investigations were supported by the Australian Research Council. The assistance of A. Johnston in acquisition of the adsorption data with the three ion-exchange resins is greatly appreciated.

SYMBOLS

a	external surface area per unit volume of adsorbent particles
a^*	total area perpendicular to the direction of diffusion
A	parameter defined by eqns. 8 and 33
B	parameter defined by eqn. 10
C	adsorbate concentration in the liquid phase
C_i	intermediate adsorbate concentration in the liquid phase at internal surface of the particles
C_0	initial adsorbate concentration in the liquid phase
C_p	adsorbate concentration in the pore fluid
C_{p0}	initial adsorbate concentration in the pore fluid
C_T	equivalent adsorbate concentration when total amount of the adsorbate in the system was assumed in the liquid phase
C^*	intermediate adsorbate concentration in the liquid phase an external surface of the particles
D_e	effective pore diffusivity
D_M	free molecular diffusivity
k_1	forward surface interaction rate constant
K_d	adsorption equilibrium constant
K_e	overall effective liquid phase mass transfer coefficient
K_f	liquid side film mass transfer coefficient
K_p	apparent pore fluid mass transfer coefficient
M	parameter define by eqn. 7
N	mass flux
q, Q	adsorbate concentration on the solid phase
q_m, Q_m	maximum solid adsorption capacity
q_0	initial adsorbate concentration on the solid phase
R_0	particle radius
R_v	volume ratio of solid phase to liquid phase
t	time
x_1	positive root of quadratic eqn. 9
x_2	the other root of eqn. 9
ε	volume fraction of liquid phase in the finite bath
ε_p	particle void fraction
λ^*	area factor $= a^*/a$
σ	ratio of the average effective diffusion path length to the particle radius R_0

REFERENCES

1 A.I. Liapis, B. Anspach, M.E. Findley, J. Davies, M.T.W. Hearn and K.K. Unger, *Biotechnol. Bioeng.*, 34 (1989) 467.
2 H.-J. Wirth, K.K. Unger and M.T.W. Hearn, *J. Chromatogr.*, 550 (1991) 383.
3 G. Jilge, K.K. Unger, U. Esser, H.-J. Schafer, G. Rathgeber and W. Muller, *J. Chromatogr.*, 476 (1989) 37.
4 R. Janzen, K.K. Unger, W. Muller and M.T.W. Hearn, *J. Chromatogr.*, 522 (1990) 77.
5 M. Hanson, K.K. Unger and G. Schomburg, *J. Chromatogr.*, 517 (1990) 269.
6 S. Hjertén, I. Zelikman, J. Lindeberg, J.-I. Liao, K.-O. Eriksson, and J. Mohammad, *J. Chromatogr.*, 481 (1989) 175.
7 M. Kawahara, H. Nakamura and T. Nakajima, *J. Chromatogr.*, 515 (1990) 149.
8 Q.M. Mao, A. Johnston, I.G. Prince and M.T.W. Hearn, *J. Chromatogr.*, 548 (1991) 147.
9 M.A. McCoy and A.I. Liapis, *J. Chromatogr.*, 548 (1991) 25.
10 B.L. Yang, M. Goto and S.M., Goto, *J. Chem. Eng. Japan*, 22 (1989) 532.
11 B.J. Horstmann, C.N. Kenney and H.A. Chase, *J. Chromatogr.*, 361 (1986) 179.
12 F.B. Anspach, A. Johnston, H.-J. Wirth, K.K. Unger and M.T.W. Hearn, *J. Chromatogr.*, 476 (1989) 205.
13 B.J. Horstmann and H.A. Chase, *Chem. Eng. Res. Des.*, 67 (1989) 243.
14 A. Johnston and M.T.W. Hearn, *J. Chromatogr.*, 512 (1990) 101.

15 G.L. Skidmore, B.J., Horstmann and H.A. Chase, *J. Chromatogr.*, 498 (1990) 113.
16 A. Johnston and M.T.W. Hearn, *J. Chromatogr.*, 557 (1991) 335.
17 H.A. Chase, *J. Chromatogr.*, 297 (1984) 179.
18 F.H. Arnold, H.W. Blanch and C.R. Wilke, *Chem. Eng. J.*, 30 (1985) B9.
19 B.H. Arve and A.I. Liapis, *AIChE J.*, 33 (1987) 179.
20 G.H. Cowan, I.S. Gosling and W.P. Sweetenham, *J. Chromatogr.*, 484 (1989) 187.
21 H. Ohashi, T. Sugawara, K. Kikuchi and H. Konno, *J. Chem. Eng. Japan*, 14 (1981) 433.
22 J.M. Smith, *Chemical Engineering Kinetics*, McGraw-Hill, New York, 3rd ed., 1981.
23 M.E. Young, P.A. Carroad and R.L. Bell, *Biotechnol. Bioeng.*, 22 (1980) 947.
24 A. Johnston, *M. (Biotech.) Thesis*, Monash University, Melbourne, 1988.
25 H.-J. Wirth, *Ph.D. dissertation*, Johannes-Gutenberg University, Mainz, 1990.
26 R.D. Whitley, K.E. Van Cott, J.A. Berninger and N.-H. L. Wang, *AIChE J.*, 37 (1991) 555.
27 I. Yarovsky, M.I. Aguilar and M.T.W. Hearn, *J. Chromatogr.*, submitted for publication.